



Article

Assessment of the Combined Charring and Coating Treatments as a Wood Surface Protection Technique

Jure Žigon *  and Matjaž Pavlič 

Department of Wood Science and Technology, Biotechnical Faculty, University of Ljubljana, 1000 Ljubljana, Slovenia

* Correspondence: jure.zigon@bf.uni-lj.si

Abstract: Flame treatment is an ancient technique for surface protection of wood. Further processing of charred wood elements depends on aesthetic and protective requirements. This study presents some general properties and weathering behaviour of the Norway spruce (*Picea abies* (L.) Karst.) and the European larch (*Larix decidua* Mill.), protected by variations of sanding, charring, charring + brushing, and coating treatments. Charring and charring + brushing reduced the original mass of the samples by up to 8% and notably changed their colour ($\Delta E^* \leq 75$). A study of chemical properties showed that charring dehydrated the wood and degraded lignin and hemicelluloses. The surface roughness of the wood after charring and charring + brushing increased by as much as 560%, while coating with waterborne acrylic high build stain had no effect on the roughness of these surfaces. The type of surface treatment of the wood did not affect the uptake of the coating in the wood samples, but the uncoated and coated spruce wood absorbed more water than larch wood. Higher water absorption was observed in the samples treated by charring, and it decreased when the char layer was removed by brushing. The film of a waterborne high build stain reduced water uptake only for surfaces treated by sanding and charring + brushing. Larch wood exhibited higher surface hardness ($E_{Hz} \leq 1.70$ MPa) than spruce wood ($E_{Hz} \leq 0.89$ MPa), with the brittle char layer reducing the determined hardness of the tested surfaces. During two years of natural weathering, the char layer was removed from the wood surface, even if the samples were additionally coated. The greatest colour changes during weathering were observed on samples treated by sanding ($\Delta E^* \leq 60$) and sanding + coating ($\Delta E^* \leq 33$), followed by samples treated with charring + brushing ($\Delta E^* \leq 10$) and samples treated with charring ($\Delta E^* \leq 9$). In summary, treating wood by charring in combination with brushing was the best wood protection technique.

Keywords: charring; coating; European larch; Norway spruce; surface; weathering; wood



Citation: Žigon, J.; Pavlič, M. Assessment of the Combined Charring and Coating Treatments as a Wood Surface Protection Technique. *Forests* **2023**, *14*, 440. <https://doi.org/10.3390/f14030440>

Academic Editor: Xinzhou Wang

Received: 9 February 2023

Revised: 17 February 2023

Accepted: 19 February 2023

Published: 21 February 2023



Copyright: © 2023 by the authors. Licensee MDPI, Basel, Switzerland. This article is an open access article distributed under the terms and conditions of the Creative Commons Attribution (CC BY) license (<https://creativecommons.org/licenses/by/4.0/>).

1. Introduction

Nowadays, many techniques for surface protection of wood exist. The modern techniques, which include the use of film-forming coatings, appeared together with the development of synthetic polymers about 150 years ago [1]. The other, more traditional techniques of wood preservation are known from the early beginning of humankind; they are nowadays gaining the attention of architects and designers for different purposes, especially for building façades [2]. The modification of wood surface with flame is one such old techniques. This technique has been used all over the world since ancient times. The method of charring is applied on wood in order to preserve wood and prolong its lifespan, to promote a certain aesthetical appearance of wood texture, or both. In Japan, the technique of wood charring is referred as “Shou Sugi Ban” or “Yakisugi” [3] and includes the unique technique of wood charring together with application of natural oils to the charred layer. Traditionally, charring is performed by exposing the wood to a flame. However, as reported in many scientific papers from recent years, charring of wood can also be performed by heating the wood samples with so-called contact heaters [4].

Exposure of wood to elevated temperatures or heating objects causes certain chemical and physical changes on the surface of the wood [5]. The extent of these changes strongly depends on the wood species [6], anatomical orientation of wood fibres [7], the level of applied temperature, and the duration of wood exposure to heat [8,9]. Generally, the volume and mass of wood start to decrease as a consequence of water evaporation from wood (at approx. 100 °C) [10]. Further loss of mass is related to the thermal decomposition of the three main polymeric components (hemicelluloses, cellulose, and lignin) and extractives [11]. Together, they form a mixture of volatile compounds in a temperature range of (150–480) °C [12]. The non-volatile part of wood undergoes further condensation and formation of intermediate products. Finally, the carbonaceous char layer, mainly consisting of pure carbon of a typical dark colour [13] in a form of a distinct pattern of micro- and macrocracks [14], is formed on the surface of wood [13,15,16]. The resulting carbonized surfaces, with a decreased presence of hydroxyl (–OH) groups, increase cellulose crystallinity and crosslinking of lignin, and contribute to the reduced equilibrium moisture content of wood, up to values as high as 20% [4]. The changes also occur in the anatomical structure of wood exposed to flame. Li et al. [17] and Kim et al. [18] found that during the charring, the tracheid cell walls gradually homogenize. Cell wall thickness also decreases by approximately 20%. Li et al. [17] also reported on oxygen dissipation, carbon enrichment, and nitrogen content fluctuation in the charred wood.

Charring shows potential as a protective treatment of wood against wood-destroying fungi [19] and fire [8,20–22]. On the other hand, it has little effect on wood infestation by subterranean termites [23]. The main advantages of the charring technique are especially the simplicity of the process and its usability in protecting wood against weathering [3]. The latter is also the reason for an increased interest in studying the properties of charred wood in recent years. The degree of protection of wood with the charred surface depends on the thickness of the carbonized layer [24]. In general, the wettability of wood with water is an important indicator in predicting how a particular wood surface is prone to absorb water. When the charred wood is exposed to rain outdoors, the char layer acts as a barrier to water penetration [25]. As reported by Morozovs et al. [13], the charred wood has lower water vapour accumulation than normal wood. Moreover, the results of Čermák et al. [4], Kymäläinen et al. [26], and Šeda et al. [27] show that surface charring notably improves the hydrophobicity of the wood surface, which is determined by water contact angle measurements, water floating test, and dynamic vapour sorption measurements. However, in case of the formed cracks in the charred layer, these can weaken the barrier function of char and do not prevent the water absorption in the underlying wood [26]. The studies of Kymäläinen et al. [28,29], performed on different charred wood species exposed to outdoor weathering, showed extensive cracking of samples, colour fading caused by the sunlight, flaking of the surface layer, and washing-off of the char by rainfall.

When used for construction purposes (e.g., for façade claddings) [21], the choice of further processing of elements mainly depends on aesthetic requirements. With respect to wooden elements with charred surfaces, the charred layer can remain as such or can be additionally removed by brushing. This technique promotes the visual difference between earlywood areas, latewood areas, and decorative-looking wood surfaces in general. The surface of the charred wooden elements can be furtherly coated with natural oils or film-forming synthetic coatings, for both decorative and protective reasons [2,16,20,30,31].

Despite many scientific reports dealing with the wettability and weathering performance of the surface charred wood, there is still a lack of reports addressing detailed water uptake abilities of this type of wood. Knowledge about the general properties and weathering performance of wood protected by a charring technique, in combination with the coating process, is missing. By reporting the results found on the two wood species most commonly used for construction purposes in Europe, the present study attempts to answer these questions. Wood samples with surfaces treated with sanding, combined charring and brushing, and sole charring were compared in terms of loss of mass due to the performed treatments, chemical properties, and ability to absorb the liquid coating (waterborne high

build stain). Together with the coated samples, the materials were microscopically analysed and tested for water uptake and indentation hardness. With the aim to test the contribution of the surface coverage with film-forming coating against natural weathering, all types of the wood samples with the treated surfaces were exposed for two years in the outdoor test field. Their performance was periodically evaluated in terms of colour changes and general visual assessment.

2. Materials and Methods

2.1. Wood Materials

The strain-grained wood, which is free from knots and other defects of Norway spruce (Sp, *Picea abies* (L.) Karst.), and European larch (La, *Larix decidua* Mill.) were used as a substrate material. The wood was obtained from local forest in Slovenia. Prior to further processing, it was stored in a room with a relative humidity (RH) of 40% and temperature 23 °C for two years. During the time of storage, the Sp wood acclimatized to an equilibrium moisture content of 8.5% and nominal density of $418.0 \text{ kg} \times \text{m}^{-3}$ (both determined gravimetrically), while the La wood reached an equilibrium moisture content of 9.2% and nominal density of $670.2 \text{ kg} \times \text{m}^{-3}$.

Wood was mechanically processed (sawed and surface planed) to the samples with dimensions of (370 × 75 × 20) mm with quarter wood grain on the larger surface (longitudinal × radial × tangential; L × R × T), as required by the standard EN 927-3 [32]. In total, 30 samples were prepared from each type of wood.

2.2. Wood Surface Treatments

Six different sets of samples were prepared from Sp and La wood, differing in type of the surface treatment. The acronyms of sample series used in the study with described surface treatment methods are listed in Table 1. After processing with surface planer, the sanded (S) samples were prepared by sanding the surfaces with sanding paper of grit P150 by using random orbital sander model BO5031 (Makita, Nagoya, Anjo, Japan). The sanded + coated (S + Co) samples were, after sanding, coated with a transparent commercial waterborne acrylic high build stain intended for protection of wood in the exterior (Belinka Exterior, Helios TBLUS d.o.o., Količevo, Slovenia). The coating was applied with amount of $(53 \pm 8) \text{ g} \times \text{m}^{-2}$ to the front and side faces of each sample by high-volume low-pressure spraying in two layers with intermediate sanding (paper grit P240). The charred + brushed (Ch + B) samples were firstly charred over the front and side faces by using a butane-propane torch and manually brushed with a steel wire brush afterwards. The preliminary experiments of monitoring with the infrared camera showed that the maximum temperature during the charring of wood samples was between (530 and 680) °C. Charring with torch was terminated when the first cracking of the wood surface was observed, while brushing was performed until the charred layer was removed (visually estimated). The charred + brushed + coated (Ch + B + Co) samples were prepared in the same way as Ch + B ones, but, after brushing, they were additionally coated in two layers. The charred (Ch) samples remained as such after charring, while the charred + coated (Ch + Co) samples were also coated in two layers after charring without prior brushing.

Table 1. The acronyms of sample series used in the study with described surface treatment methods.

Wood Type	Surface Treatment Method and Given Acronym					
	Sanded	Sanded + Coated	Charred + Brushed	Charred + Brushed + Coated	Charred	Charred + Coated
Spruce	Sp-S	Sp-S + Co	Sp-Ch + B	Sp-Ch + B+Co	Sp-Ch	Sp-Ch + Co
Larch	La-S	La-S + Co	La-Ch + B	La-Ch + B+Co	La-Ch	La-Ch + Co

Four samples with a certain surface treatment were used in the natural weathering test (described in Section 2.7) and one was used for all the other studies, including short-term uptake analyses (Section 2.5) and for determination of surface indentation hardness (Section 2.6).

Recording of Samples Mass Loos

Mass loss (m_L) based methods may be utilized to detect the progress of charring [33]. Moreover, with the aim of precise monitoring of the samples m_L during each type of surface treatment process, the samples masses were measured after each preparation step. The m_L of the samples acclimatized at room conditions due to different preparation of the surfaces was calculated as (Equation (1)):

$$m_L = \left(\frac{m_0 - m_{S, Ch+B \text{ or } Ch}}{m_0} \right) \times 100 [\%], \quad (1)$$

where $m_{S, Ch+B, \text{ or } Ch}$ [g] represent the mass of the samples after being S, Ch + B, or Ch and m_0 [g] represents the initial mass of these samples.

2.3. Chemical Analysis of Surfaces

The chemical properties of S, Ch + B, and Ch wood surfaces were investigated with attenuated total reflection Fourier transform infrared (ATR-FTIR) spectrometer Spectrum Two (PerkinElmer Inc., Waltham, MA, USA). The information about the chemical properties were gained from each type of treated wood surface at 3 locations in the middle of the samples, including the early- and latewood structure. FTIR spectra recorded (16 scans) in a wavelength region from (600 to 4000) cm^{-1} at a resolution of 0.5 cm^{-1} . The relevant absorption bands were elucidated with Spectrum V.10.5.3 software (PerkinElmer Inc., Waltham, MA, USA).

2.4. Microscopic Investigations of Surfaces

2.4.1. Analysis of Microscopic Structure

The microscopic structures of surfaces and cross-sections of the samples were analysed with digital light microscope DSX 1000 (Olympus, Tokyo, Japan) at 10 \times magnification. The cross-sections were smoothed on a sledge microtome SM2010R (Leica Microsystems GmbH, Wetzlar, Germany) before observations.

2.4.2. Surface Roughness Measurements

The influences of the different treatment methods on the surface morphology of the samples were investigated with a LEXT OLS5000 confocal laser scanning microscope (CLSM, Olympus, Tokyo, Japan). The roughness of three spots of (11.8 \times 11.8) mm was measured at 5 \times magnification with a laser (light wavelength 405 nm). The changes in surface morphology due to sanding, charring, charring and brushing, and coating processes were measured on the same locations of the studied sample before each treatment and after it. OLS50-S-AA software (Olympus) was used to provide an arithmetic mean height of the surface.

2.5. Short-term Water and Coating Uptake Analysis

Short-term uptake analysis was performed on a Krüss Processor Tensiometer K100 (Krüss, Hamburg, Germany) at room temperature and RH of 40%. Twenty samples with dimensions (20 \times 15 \times 15) mm (L \times R \times T) were cut out of one larger sample of each type. Except the treated surface, all the other five surfaces of each sample were sealed by immersion in a transparent nitrocellulose lacquer (Helios TBLUS d.o.o.). The surface tension of water and the liquid coating were determined according to the Du Noüy ring method [34] and used as input before the measurements. By immersing the samples into the deionized water and waterborne coating with the treated surface facing the liquid, the sample mass increase and the sorption curves were determined with Krüss LabDesk

software. Each sample was first immersed in the liquid to a depth of 3 mm at a rate of $6 \text{ mm} \times \text{min}^{-1}$. Then, the measurement of mass increase began (detection force sensitivity was 0.001 N). Liquid uptake into the immersed samples was monitored for 200 s.

2.6. Determination of Indentation Hardness

When using wooden elements for constructional building purposes, the hardness of wood surface has an important role for elements to withstand the damage caused by the extreme weather inconveniences, for example, the fall of hail. The hardness of the treated wood surfaces was determined with one-cycle indentation test applied on one ($20 \times 75 \times 20$) mm (L \times R \times T) sample of each type. The tests were performed on the Micro Combi Tester (MCT³, Anton Paar GmbH, Graz, Austria) by using a certified spherical steel indenter (6 mm in diameter). The indenter was pressed in the samples at 6 different spots in a line, with a distance between two adjacent spots of 10 mm. The load of indentation linearly increased from 2 mN to 10,000 mN, with a loading rate of $5000 \text{ mN} \times \text{min}^{-1}$. The maximal load was maintained for 1 s and then released with an unloading rate of $5000 \text{ mN} \times \text{min}^{-1}$. The penetration depth P_d [μm] of the indenter in the sample with respect to the applied normal load F_n [mN] was monitored with acquisition rate of 10 Hz. The response of the tested samples to indentation was quantified by fitting the load curve between 10% and 98%. The elastic modulus E_{Hz} [MPa] was quantified by the Indentation software provided with the MCT³ (version 10.0.9, Anton Paar GmbH), calculated on the basis of Hertz analysis method [35], following relation (Equation (2)):

$$F_n = \frac{4}{3} \times \frac{E_{Hz}}{1 - \nu^2} \times \sqrt{R} \times P_d^{\frac{3}{2}}, \quad (2)$$

where ν is the Poisson's ratio of the sample (set to 0.3) [36] and R is the indenter radius (3 mm).

2.7. Natural Weathering Test

The natural weathering was performed in accordance with EN 927-3 (2019) [32] in the field test site of the Department of Wood Science and Technology, Ljubljana, Slovenia (N $46^\circ 02' 55.4''$, E $14^\circ 28' 44.6''$, altitude 293 m). The exposure period lasted 24 months in total: from the 15 January 2021 to the 15 January 2023. The climatic data were collected by the weather station Vantage Pro (Davis Instruments Corporation, Hayward, USA). Three samples of each type of wood and each type of surface treatment were placed on the inclined (45°) exposure racks facing towards the equator, and the fourth sample (unexposed reference) was kept in the dark at room conditions, as prescribed by the standard SIST EN ISO 2810 [37]. Besides the colour changes (described in Section 2.8), the exposed samples were visually assessed according to SIST EN 927-3 [32] and other specific standards in each inspection period: cracking (SIST ISO 4628-4 [38]), flaking (SIST ISO 4628-5 [39]), and disfigurements caused by fungal or algal growth (SIST EN 16492 [40]).

2.8. Monitoring of Colour Changes

The colour of the samples was measured before and after surface treatment of the wood samples and after the following periods of natural weathering: 1, 3, 6, 9, 12, 15, 18, 21, and 24 months. The SP62 spectrophotometer (X-Rite, Grand Rapids, MI, USA) with the D65 light type was used to measure the colour of the inspected surfaces at 5 random spots, following the CIELAB colour space coordinate system [41]. The values of changes in colour of the sample surfaces (ΔE^*) were calculated according to Equation (3):

$$\Delta E^* = \sqrt{(\Delta L^*)^2 + (\Delta a^*)^2 + (\Delta b^*)^2}, \quad (3)$$

where ΔL^* , Δa^* , and Δb^* represent the changes in the values of luminance (L^* , ranging from 0—totally black to 100—total white) and chromatic coordinates a^* ($+a^*$ —reddishness, $-a^*$ —greenishness) and b^* ($+b^*$ —yellowing, $-b^*$ —blueness). In addition, the samples were

scanned with optical scanner S2400 plus (Mustek Europe B.V., Oosterhout, The Netherlands) with 600 DPI resolution.

3. Results and Discussion

3.1. Mass Loss Due to Surface Treatments

Each type of surface treatment caused a mass decrease of wood samples. The results are presented in Figure 1. The removal of a thin surface layer with sanding resulted in a m_L of $(0.3 \pm 0.0)\%$ for Sp wood samples and of $(0.2 \pm 0.1)\%$ for La wood samples. A higher m_L for Sp wood than for La wood is due to the coincidence of Sp wood having a lower wood density [42]. The charring of wood surfaces caused a notable m_L for both types of wood. In the present case, the combustion of surface layer for Sp-Ch wood and La-Ch wood resulted in m_L of $(7.3 \pm 2.7)\%$ and $(5.6 \pm 0.6)\%$, respectively. The removal of the charred layer by brushing caused a similar m_L on both types of wood and sole charring, and accounted to $(6.9 \pm 1.0)\%$ for Sp-Ch + B wood and to $(5.4 \pm 1.0)\%$ for La-Ch + B wood. This similarity in m_L indicates that the carbonized charred layer, with its high porous structure and low density, contributed little to the total mass of the samples. The results are also in the range of wood diversity between the samples.

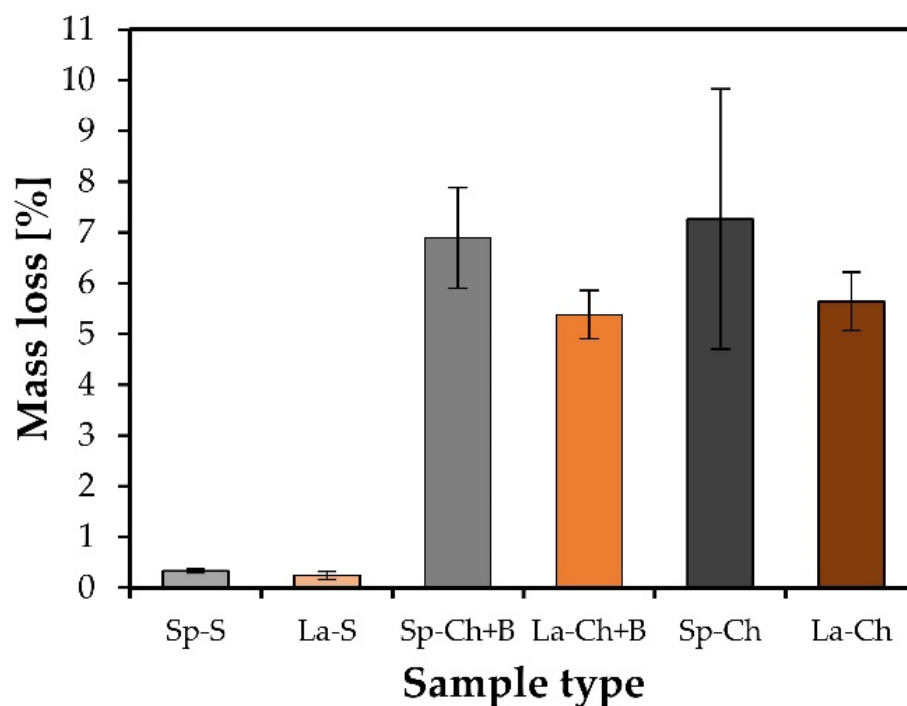


Figure 1. Mass loss of Sp and La wood samples after different surface treatments.

3.2. Colour Changes Caused with Surface Treatments

Similar to m_L , each type of surface treatment also caused the changes in colour of Sp and La wood (Figure 2). The sanding alone perceptibly ($\Delta E^* \geq 2$) [43] changed the colour of both wood species: $\Delta E^* = 2.0$ for Sp-S and $\Delta E^* = 2.7$ for La-S. In terms of the change in lightness, only sanding made the surfaces of wood lighter ($\Delta L^*_{Sp-S} = 1.0$; $\Delta L^*_{La-S} = 1.74$). The presence of the coating film on the surface additionally promoted the change of colour of samples after sanding: $\Delta E^* = 10.1$ for Sp-S + Co and $\Delta E^* = 8.5$ for La-S + Co. The surface treatments, including charring, darkened the surfaces of wood (e.g., $\Delta L^*_{Sp-Ch+B} = -69.2$; $\Delta L^*_{La-Ch+B} = -55.3$). Moreover, charring and charring + brushing comparably changed the colour of Sp wood ($\Delta E^*_{Sp-Ch} = 73.5$; $\Delta E^*_{Sp-Ch+B} = 72.2$) and La wood ($\Delta E^*_{La-Ch} = 56.0$; $\Delta E^*_{La-Ch+B} = 61.1$).

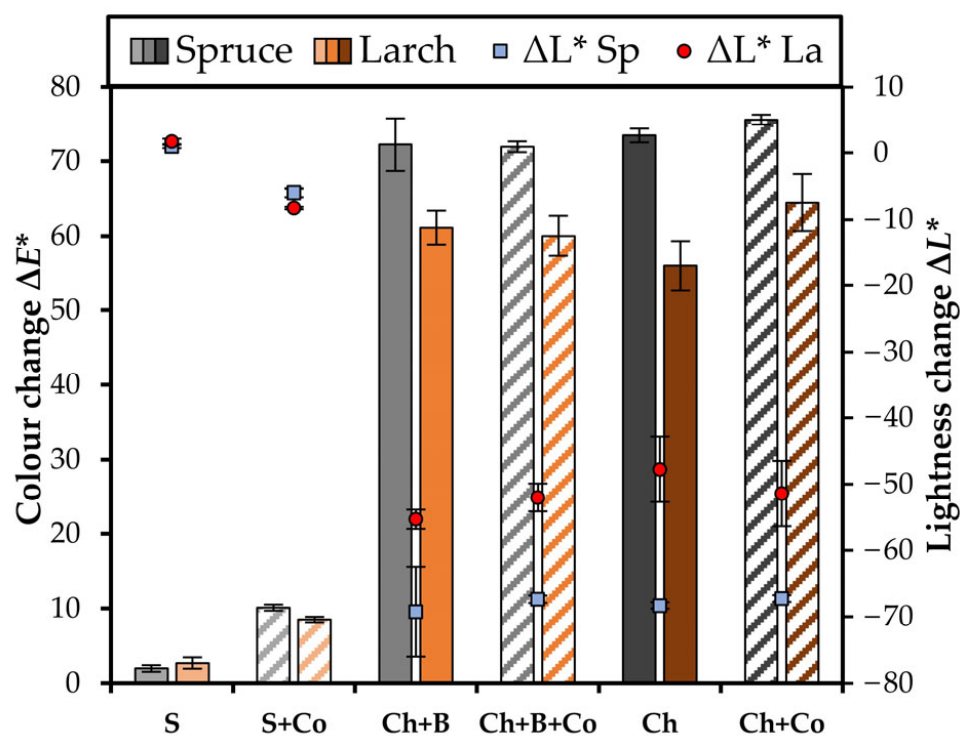


Figure 2. Colour and lightness changes on Sp and La wood samples caused by different surface treatments. The slashed columns present the samples with applied coating.

3.3. FTIR Spectra

The surfaces of Sp-S and La-S wood exhibited comparable FTIR spectra that are typical for softwoods (Figure 3). By charring and brushing of wood, several chemical properties of the surfaces were changed. The increased peak in the range of $(1030\text{--}1060)\text{ cm}^{-1}$, representing C–O, aliphatic C–O–C, and hydroxyl (–OH) functional groups, signalled the promotion of oxygenation of cellulose and lignin [44–46]. The peak at 1100 cm^{-1} , representing aliphatic ether (C–O–) and alcohol (C–O) stretching in cellulose and hemicelluloses, intensified due to higher stability of carbohydrates (particularly cellulose) compared to lignin [24,25]. In general, the guaiacyl and syringyl structural units in lignin are more susceptible to temperature and can be eliminated during pyrolysis [47]. The intensified peak at 1200 cm^{-1} signalled deformation of –OH functional groups [48]. The intensified peak at 1580 cm^{-1} signalled the promoted presence of aromatic skeletal vibration typical of syringyl units in lignin [45,49]. In contrast, the peak at 1640 cm^{-1} (conjugated C=O bonds coupled with C=O stretching in various groups) decreased, which can be interpreted as lignin degradation combined with the formation of new carbonyl (C=O) functional units [50]. The intensity of the peak at 1740 cm^{-1} presents stretching in non-conjugated C=O groups and was slightly reduced. This reflects changes in various functional groups in lignin and hemicelluloses (carbonyls, esters, ketones, aldehydes, and carboxylic acids). Traoré et al. [45] assigned this to the complex cleavage of bonds in lignin, leading to generation of water-soluble products, and finally, to chromophoric groups like carboxylic acids (–COOH), quinines, or hydroperoxides. The diminished intensity of the peaks at $(2850\text{ and }2920)\text{ cm}^{-1}$ signalled reduced C–H and –OH stretching and could be attributed to crystallinity altering of the cellulose [47].

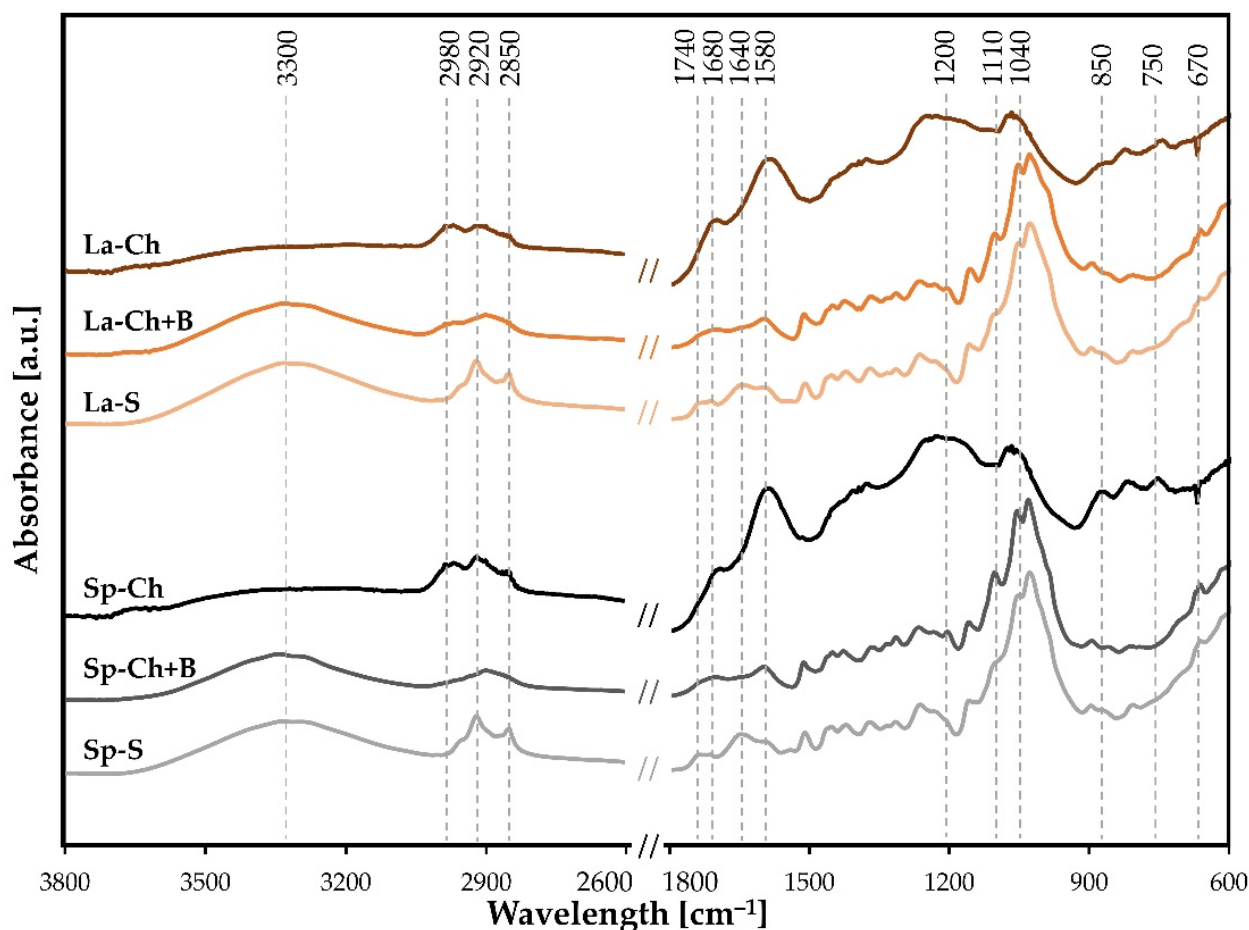


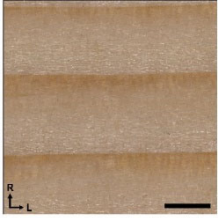

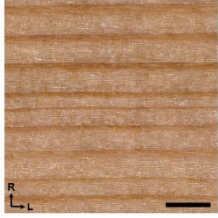

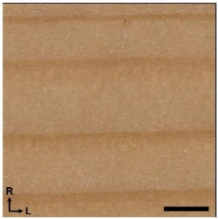

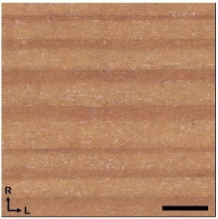
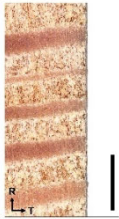
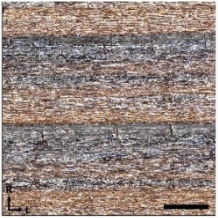

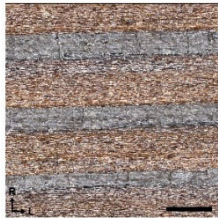
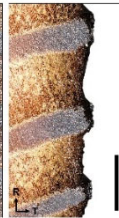
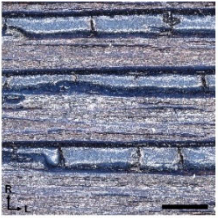

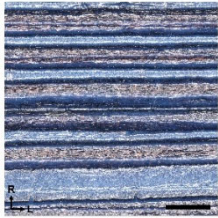

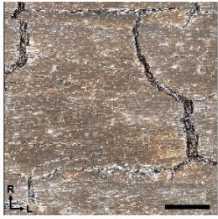

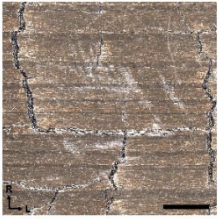

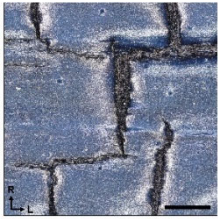

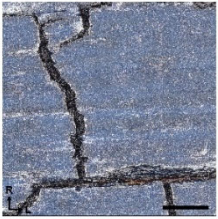

Figure 3. FTIR spectra recorded on Sp and La wood with differently treated surfaces.

The FTIR spectra acquired on the Ch wood surfaces were very similar to those reported by Constantine et al. [51], recorded for charcoal. The disappearance of the peak at 670 cm^{-1} signalled the general degradation of the cellulose and lignin [47]. A newly formed peak at 750 cm^{-1} indicated a higher presence of aromatic C–H bonds on the benzene ring in the charred layer [48,52]. An intensified peak at 850 cm^{-1} indicated deformation of C–H bonds of glucose ring in cellulose [53]. The intensity of the peaks between (1325 and 1375) cm^{-1} , associated to C–H vibration in polysaccharides, hemicelluloses, and lignin components, diminished due to the degradation of the wood components with charring [47]. A high, intense peak at around 1580 cm^{-1} was notably enlarged. This was attributed to the degradation of C=C bonds in aromatic rings in lignin and the formation of –COOH, ketones (C=O), and other aromatic compounds, originating from the elimination of hydrogen and oxygen of aliphatic compounds during pyrolysis [47]. As for S wood, the peaks at (2850 and 2920) cm^{-1} were associated with methoxyl (–CH₃) groups stretching and aliphatic C–H stretching of the lignin [47,54]. A newly formed peak at 2980 cm^{-1} indicated C–H stretching vibrations derived from methyl (CH₃), methylene (–CH₂–), and methine (=CH–) groups [51]. Finally, the decreased intensity of the broad peak between (3320 and 3400) cm^{-1} is attributed to the dehydration (loss of –OH groups) of wood [44,55].

3.4. Surface Microscopic Structure

The investigation of wood samples with digital light microscope revealed the microscopic structural features of the treated wood surfaces, as observed from the top view and cross-sections (Table 2). At the same time, monitoring of the surfaces with CLSM showed the relations between the type of wood, the type of surface treatment, and the values of arithmetic mean height (Figure 4).

Table 2. Microscopical images of Sp and La wood samples with differently treated surfaces from the top view (left images) and cross-section (right images). The length of the scale bars is 2 mm.

Surface Treatment	Type of Wood			
	Spruce		Larch	
S				
S + Co				
Ch + B				
Ch + B + Co				
Ch				
Ch + Co				

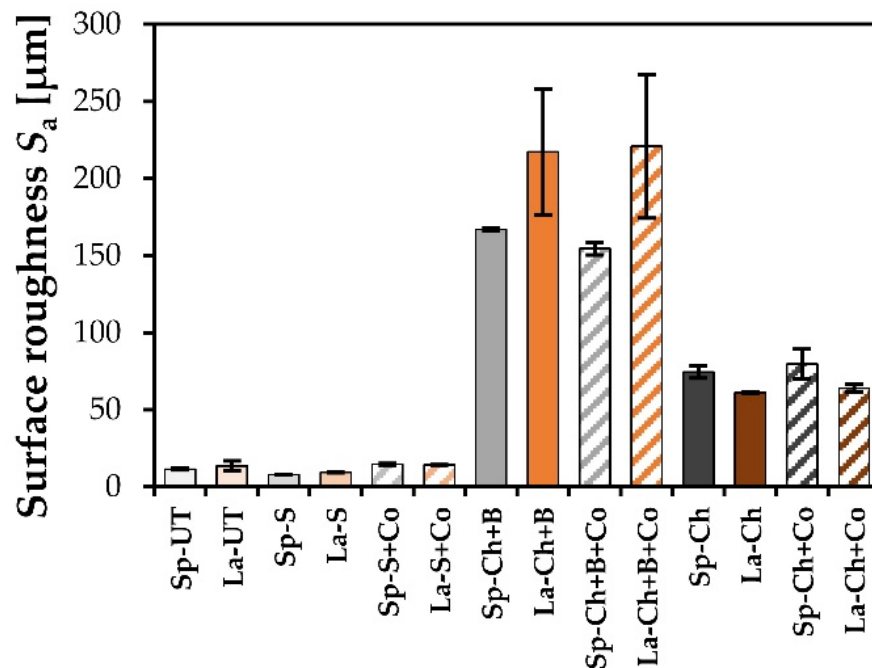


Figure 4. Surface (average of 3 spots of $[11.8 \times 11.8]$ mm) roughness of Sp and La wood samples with differently treated surfaces.

The sanding of wood samples made the surfaces smoother, since the surface roughness of both Sp and La wood decreased by -31% in comparison to the surface roughness of untreated wood. The film thickness of the coating system was most easily measured on S + Co wood surfaces due to their flatness. The coating film thickness on Sp-S + Co wood was $(55.6 \pm 4.3) \mu\text{m}$. On La-S + Co wood, it was $(62.2 \pm 11.2) \mu\text{m}$. Meanwhile, the roughness of S samples increased with coating application (Sp-S + Co for 86% and La-S + Co for 52%) due to rise of wood fibres, which is a typical phenomenon when using waterborne coatings on wood [56]. Brushing of wood after charring mostly removed the earlywood structure. Accompanied formation of about $(0.5\text{--}0.7)$ mm deep grooves considerably (for $14\text{--}15\times$) raised the roughness of the wood surfaces. Application of coating on Ch + B wood surfaces did not influence their surface roughness. The charring of wood generally resulted in complete in-depth (about 1 mm) carbonization of the surface layer. In this case, the simultaneous thermal expansion and softening of wood material during charring put the surface under extreme tension. Immediately after exposure to heat, the shrinkage of the wood exceeded its strength in the L direction, which resulted in the formation of cracks perpendicular to the wood grain [8,14]. These cracks contributed to increased surface roughness of Ch wood of 558% (Sp) or 354% (La) compared to untreated wood, respectively. Under the char layer, the thermally modified transition layer [57] or pyrolysis zone [58] with a thickness of about 1 mm could be observed beneath the intact wood. The coating of Ch wood surfaces did not influence their surface roughness, and the cracks remained partially unfilled with the coating.

3.5. Uptake of Liquids

3.5.1. Uptake of Coating in Wood

The curves of wood samples mass increase, detected during 200 s of coating uptake measurements in Sp and La wood with differently treated surfaces, are shown in Figure 5. A relatively comparable amount of the coating was taken up by Sp and La wood samples: both ranged from $(0.066 \pm 0.007) \text{g} \times \text{m}^{-2}$ to $(0.077 \pm 0.010) \text{g} \times \text{m}^{-2}$. The differences in coating uptake were too small to detect any influence of type of wood surface treatment.

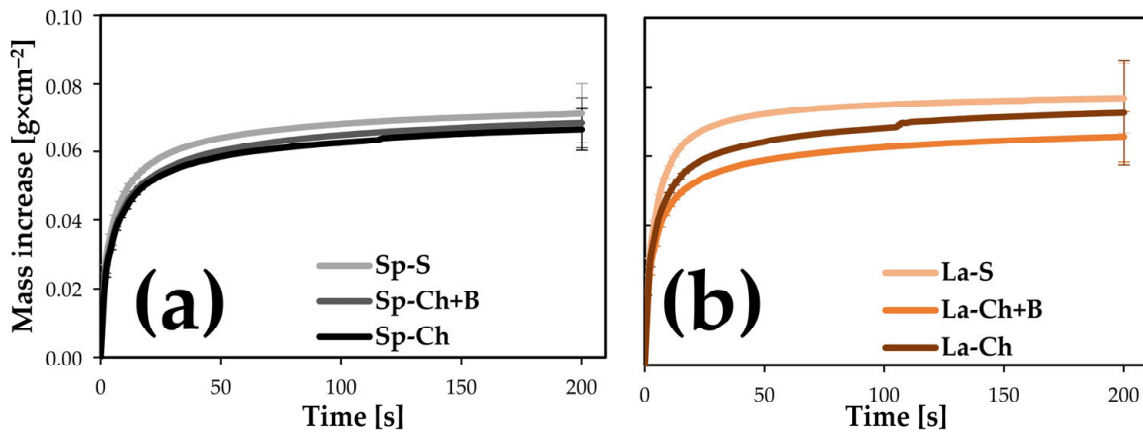


Figure 5. Coating uptake in (a) Sp and (b) La wood with differently treated surfaces.

3.5.2. Uptake of Water in Treated Wood

The detected uptake of water in wood in the present study was about five times smaller than in other studies [59] (Figure 6). Here, surfaces with R orientation of the wood fibres were immersed. The capillary forces in these are smaller than through the cross-sections of wood. Moreover, lower mass increases were detected in case of immersions of samples in water than in coating due to the higher density of coating ($1.10 \text{ g} \times \text{cm}^{-3}$) than of water ($1.00 \text{ g} \times \text{cm}^{-3}$).

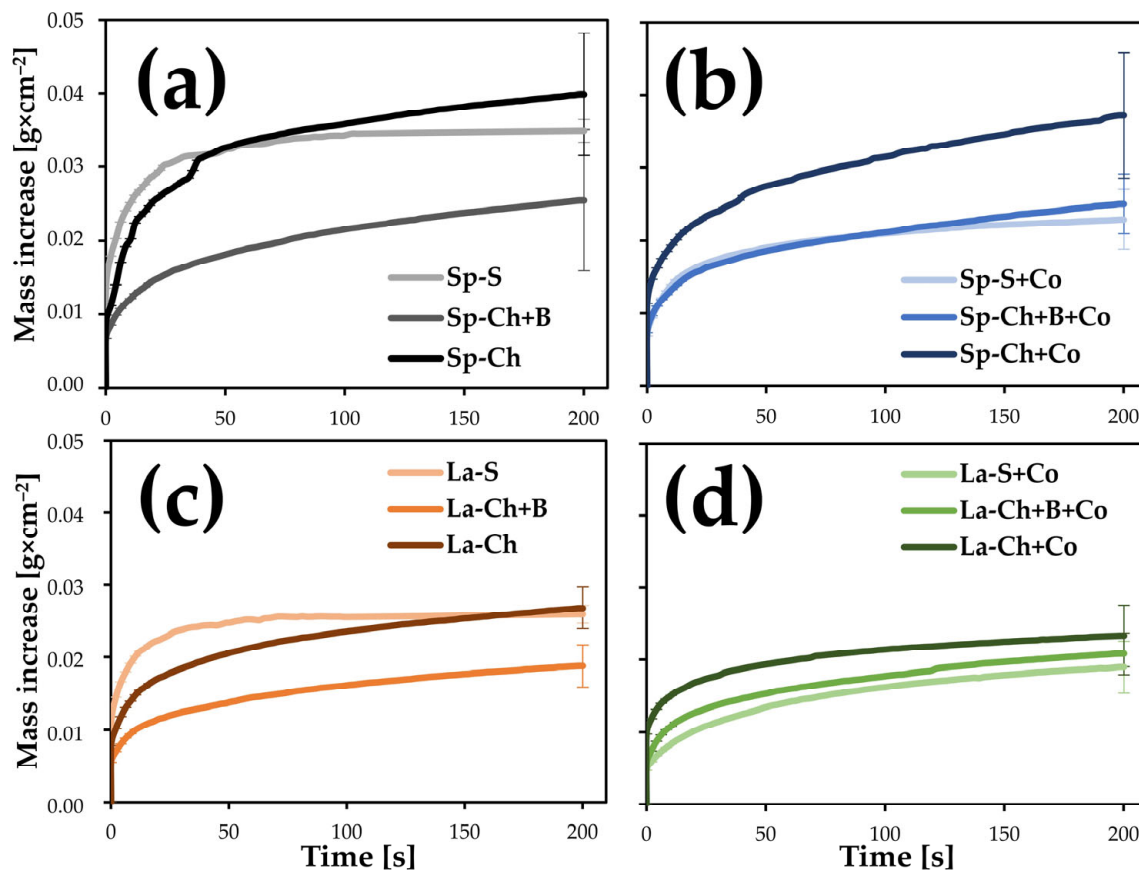


Figure 6. Water uptake in (a,b) Sp and (c,d) La wood with differently treated surfaces.

In general, the Sp wood samples absorbed more water than the La wood samples, which is related to the differences in density, anatomical structure, and chemical properties between these two wood species. The highest amount of water was absorbed by the Ch

samples (Sp-Ch $[0.040 \pm 0.008] \text{ g} \times \text{cm}^{-2}$, La-Ch $[0.027 \pm 0.003] \text{ g} \times \text{cm}^{-2}$). This could be related to the presence of cracks on the surface, which acted as larger capillaries for water uptake. In addition, the layer of coating did not noticeably prevent water uptake (Sp-Ch + Co $[0.037 \pm 0.009] \text{ g} \times \text{cm}^{-2}$, La-Ch + Co $[0.023 \pm 0.004] \text{ g} \times \text{cm}^{-2}$) because the coating did not fill these cracks, as shown in the microscopic images in Section 3.4. The water uptake in the other sample types was comparable. The S wood surfaces showed slightly different mass gain dynamics at the beginning of the measurements. At the end of measurements, the values reached $(0.035 \pm 0.002) \text{ g} \times \text{cm}^{-2}$ (Sp-S) and $(0.026 \pm 0.001) \text{ g} \times \text{cm}^{-2}$ (La-S). The lowest water uptake was measured on S + Co surfaces, namely $(0.023 \pm 0.04) \text{ g} \times \text{cm}^{-2}$ on Sp-S + Co and $(0.019 \pm 0.04) \text{ g} \times \text{cm}^{-2}$ on La-S + Co. Charring and brushing of the wood surfaces contributed to decreased water uptake (Sp-Ch + B $[0.025 \pm 0.004] \text{ g} \times \text{cm}^{-2}$, La-Ch + B $[0.019 \pm 0.003] \text{ g} \times \text{cm}^{-2}$) in comparison to S wood. It seems that, despite the increased surface roughness and consequently increased specific surface area where water molecules could attach and penetrate further into the wood, the thermally modified layer under the char layer decreased the affinity of wood to absorb water. The coating on Ch + B wood surfaces did not appear to additionally reduce the mass increase of the samples due to water uptake (Sp-Ch + B + Co $[0.025 \pm 0.004] \text{ g} \times \text{cm}^{-2}$, La-Ch + B + Co $[0.021 \pm 0.004] \text{ g} \times \text{cm}^{-2}$). Once again, it was shown that char layer does not act as wood protector and has little effect on diminishing underlying wood moisture [13].

3.6. Indentation Hardness

The curves of P_d in relation to F_n applied on the surfaces of Sp and La wood are shown in Figure 7. The maximal P_d and the calculated values of E_{Hz} are listed in Table 3. In general, due to higher density of La wood, the indentation body penetrated deeper in Sp samples than in La samples. Consequently, the E_{Hz} of La wood was higher also than that of Sp wood. For both wood species, the E_{Hz} on S, S + Co, Ch + B, and Ch + B + Co surfaces were comparable: for Sp, they were [(0.52, 0.89, 0.52, 0.43) MPa]; for La, they were [(1.70, 1.41, 1.65, 1.69) MPa]. This indicates that the hardness of wood surface is mainly dependent on the presence and share of the latewood. The earlywood on Ch + B surfaces was removed, but the remaining latewood still contributed to hardness comparable to those on S wood. In contrary, the wood with Ch surfaces exhibited notably higher P_d (488.83 μm on Sp-Ch + Co; 155.48 μm on La-Ch + Co) or lower E_{Hz} (0.06 MPa on Sp-Ch + Co; 0.63 MPa on La-Ch + Co), respectively. The reason for this is the significantly lower density and brittle structure of the char layer [33].

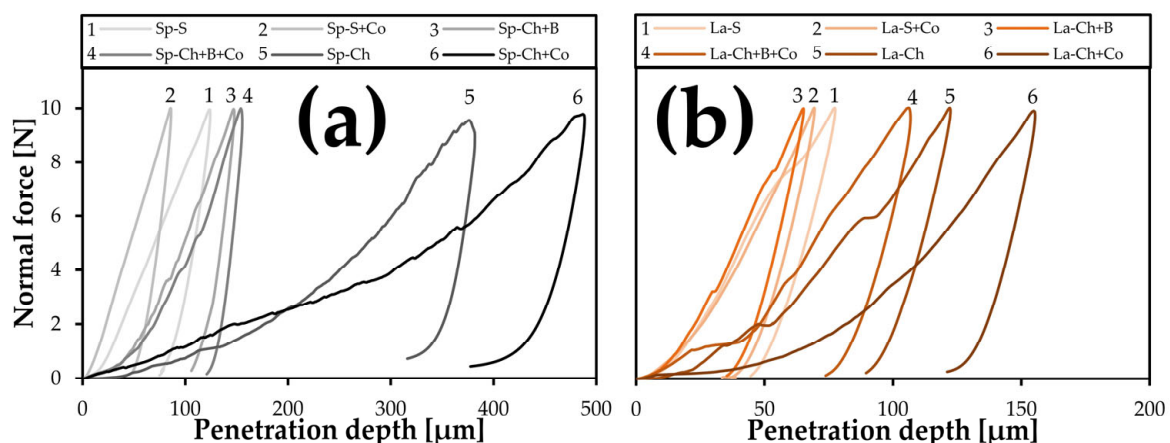


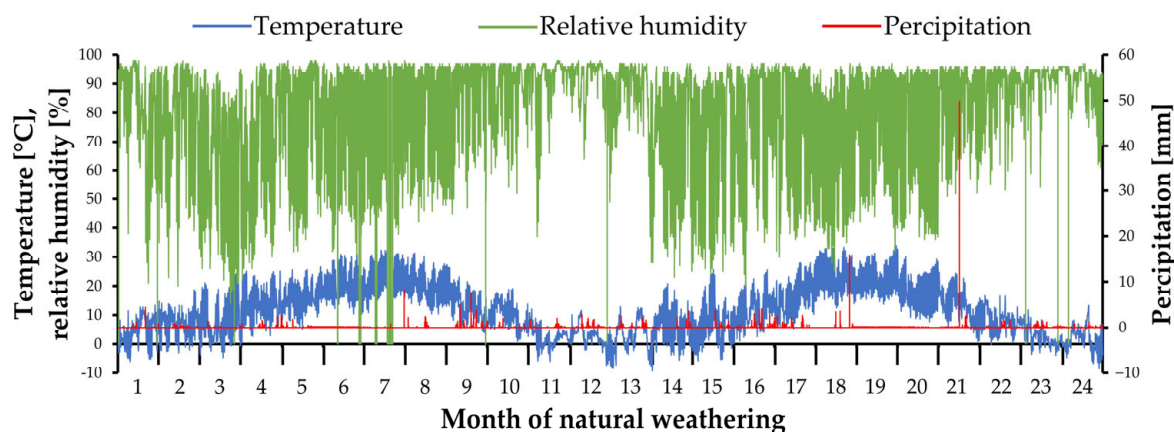
Figure 7. The curves of P_d in relation to F_n applied on (a) Sp and (b) La wood samples with differently treated surfaces. Note a different span of the P_d on x-axis between (a,b).

Table 3. The maximal P_d and the calculated values of E_{Hz} on Sp and La wood with differently treated surfaces.

Wood Type	Surface Treatment	P_d [μm]		E_{Hz} [MPa]	
		Avg.	St. dev.	Avg.	St. dev.
Sp	S	124.38	26.34	0.52	0.20
	S + Co	86.21	27.54	0.89	0.39
	Ch + B	147.90	37.88	0.52	0.19
	Ch + B + Co	155.62	19.47	0.43	0.10
	Ch	384.36	62.20	0.13	0.03
	Ch + Co	488.83	32.88	0.06	0.02
La	S	77.59	41.13	1.70	1.39
	S + Co	69.50	19.81	1.41	0.55
	Ch + B	65.31	23.20	1.65	0.71
	Ch + B + Co	106.93	49.99	1.69	1.17
	Ch	122.48	4.41	0.69	0.15
	Ch + Co	155.48	33.37	0.63	0.18

3.7. Changes Caused with Natural Weathering

The data of the precipitation, air temperature, and RH collected by the weather station during the period of natural weathering are shown in Figure 8. The average temperature was 11.1 °C, the total precipitation was 1886 mm, and the RH was 80%.

**Figure 8.** On-site data of the precipitation, air temperature, and relative humidity in the weathering period.

The evolution of colour changes ΔE^* on Sp and La wood with differently treated surfaces during exposure to natural weathering, together with the images showing the samples appearance before the exposure and in each monitoring period, are presented in Figure 9. The most severe changes in colour were observed on S samples (Figure 9a). The appearance of these samples turned to dark grey during weathering, reaching ΔE^* values of (56.6 ± 3.2) for Sp-S wood and (52.2 ± 1.6) for La-S wood after 24 months of exposure. On coated samples (Sp-S + Co and La-S + Co), the first changes ($\Delta E^* \approx 6$) were already observed after the first month of weathering. The coating film started to crack after 6 months of exposure (Figure 9b). After 9 months, the first flaking and consequent biological attack were detected here. In general, the ΔE^* on Sp-Ch + B samples was around 10. It was around 4 on La-Ch + B samples during the entire time of weathering (Figure 9c). The coating film on Sp-Ch + B + Co and La-Ch + B + Co samples started to crack and flake after 6 or 9 months of weathering, respectively. This raised the colour change up to 25, which decreased to a final value of about 16 when a large part of the coating was removed from the surface (Figure 9d). No biological attachment was detected on Ch + B + Co samples, which was attributed to the partially carbonized substrate. The smallest colour changes were observed on Ch and Ch + Co samples, where, after 24 months of weathering, ΔE^*

accounted to 3 and 9, respectively (Figure 9e,f). The rainfalls mostly wash off the char layer from Ch samples, which is reflected in the change of surface colour. Such non-stability of the char layer presented a weak underlying substrate for the coating film, which both peeled and flaked together during natural weathering. However, as before, no biological attachments were detected on both Ch and Ch + Co samples.

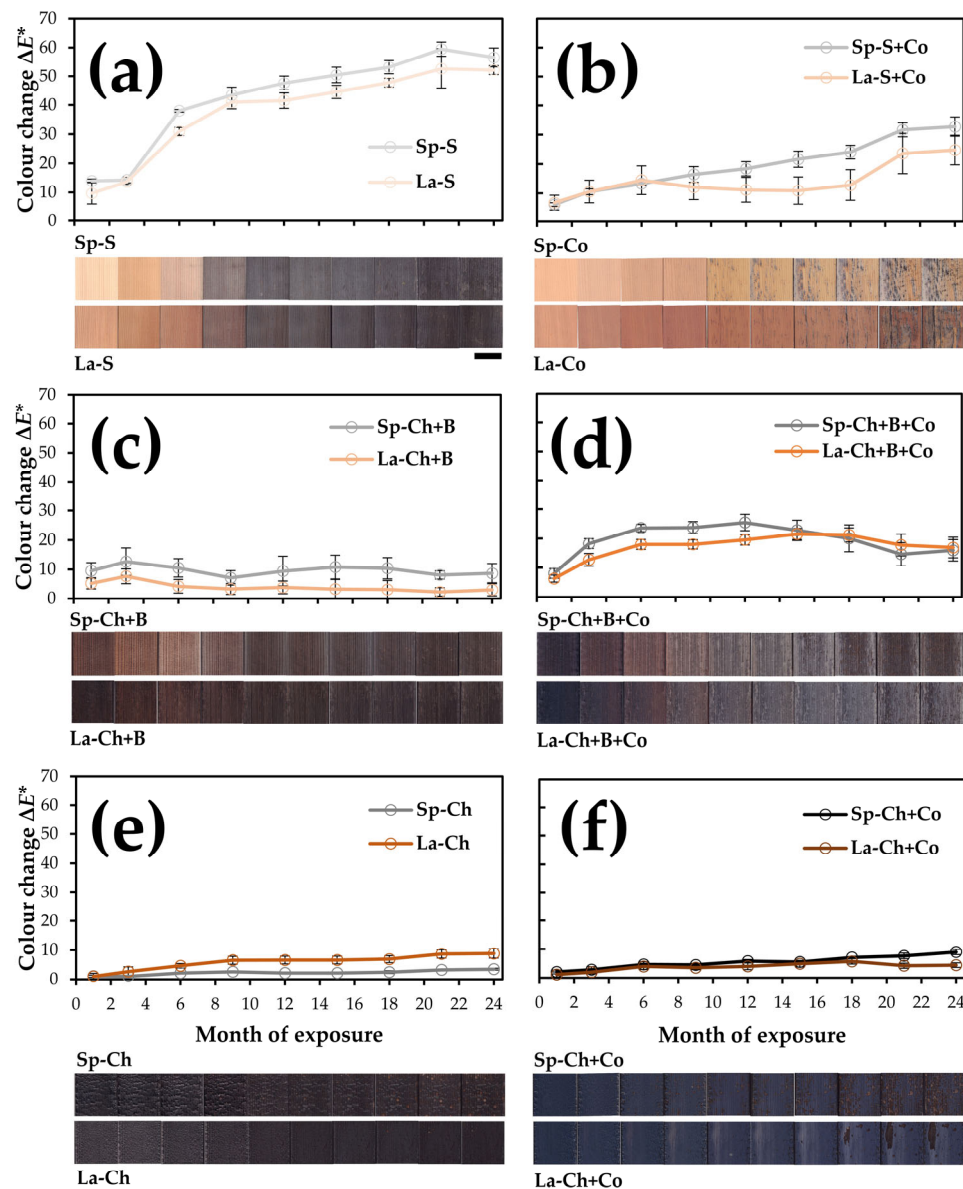


Figure 9. The evolution of colour changes ΔE^* on Sp and La wood with differently treated surfaces during exposure to natural weathering: (a) Sp-S and La-S, (b) Sp-S + Co and La-S + Co, (c) Sp-Ch + B and La-Ch + B, (d) Sp-Ch + B + Co and La-Ch + B + Co, (e) Sp-Ch and La-Ch, and (f) Sp-Ch + Co and La-Ch + Co. The images show the changes of appearance of the samples before the exposure and in each monitoring period. The length of the scale bar is 50 mm.

The images of the entire samples before the exposure to natural weathering and the images of samples taken in each monitoring period are shown in Table S1 in Supplemental Materials. The results of visual assessment of cracking, flaking, and disfigurements, detected in each inspection period, are also presented in Tables S2–S4 in Supplemental Materials.

A few detailed observations of damage on samples after two years of exposure to natural weathering are shown in the images in Figure 10. The hail in the period between May and July 2021 caused the cracks in surface systems. For example, this is seen on

Sp S + Co samples (Figure 10a). These cracks presented the entry point for mould and blue-stain fungi to infect the wood under the coating film. The hail, heavy rain, snow, wind, temperature changes, sunlight irradiation, and the accompanied dimensional changes of the surface structure caused the removal of the charred layer of Ch wood samples (Figure 10b). This could not be prevented by the additional coating layer as observed on Ch + Co (Figure 10c) and Ch + B + Co (Figure 10d) wood samples. A good indicator of the harsh conditions during the two-year exposure to natural weathering was the presence of cracks and flaking of the coating film, accompanied with the biological attack on S + Co samples (Figure 10e). Although the resistance of the studied materials here refers to resistance against development of mould and blue-stain fungi, the positive effect of wood charring on resistance against decay fungi has also been reported by Machová et al. [8].

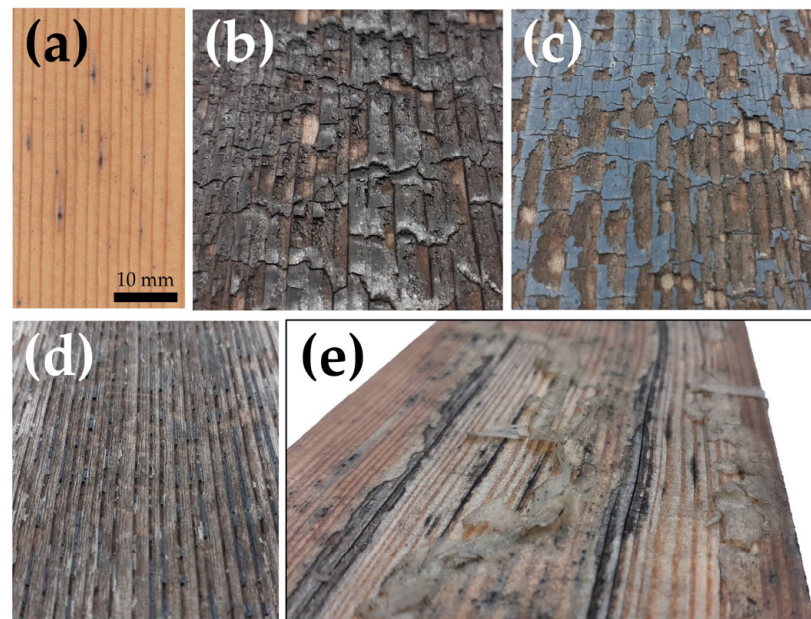


Figure 10. Detailed images of damage on samples after two years of exposure to natural weathering: (a) cracks in coating film on Sp-S + Co sample caused by hail, (b) partially removed charred layer on Sp-Ch sample, (c) partially removed charred layer on Sp-Ch + Co sample, (d) partially removed coating film on La-Ch + B + Co sample and (e) presence of cracks, biological attack, and flaked coating film on La-S + Co samples.

4. Conclusions

The study revealed some general properties and weathering behaviour of samples of two softwood species with uncoated and coated surfaces previously treated by sanding, charring, or combined charring and brushing. With sole charring and charring combined with brushing, the samples lost up to 8% of their original mass and experienced significant colour changes ($\Delta E^* \leq 75$). Charring resulted in dehydration of the wood and degradation of lignin and hemicelluloses. Both charring and charring combined with brushing increased the surface roughness of the wood by 560% (Sp) and 350% (La), respectively, compared to untreated wood, while the presence of a coating on these surfaces had no effect on their roughness. Differences in the uptake of coatings in wood samples depending on the type of surface treatment were not found. On the other hand, the Sp wood generally absorbed more water than the La wood. Higher water absorption was observed in the samples treated with charring, while removal of the char layer by brushing contributed to lower water uptake. The film of a waterborne high build stain only reduced water uptake for surfaces treated by sanding and charring in combination with brushing. With values of $E_{Hz} \leq 1.70$ MPa, La wood generally exhibited greater surface hardness than Sp wood ($E_{Hz} \leq 0.89$ MPa). The lower density and brittle structure of the char layer reduced the detected hardness of the tested wood surfaces. As was also evident during the natural

weathering of the samples, the char layer could not resist weather influences from being removed from the surface of the wood samples, even when the samples were additionally coated. As far as the colour changes during natural weathering are concerned, these were greatest for the samples treated by sanding (ΔE^* up to 60) and sanding in combination with coating (ΔE^* up to 33). Considering the colour changes, samples treated with charring and brushing (ΔE^* less than 10) and samples treated with charring (ΔE^* up to 9) better withstand the weathering. The coating film on such samples was disappearing together with the flaking of the underlying charred wood structure. Interestingly, partially or completely carbonized wood surface showed no biological attack during natural weathering. In summary, the results and observations after natural weathering showed that the samples treated with charring in combination with brushing are the most resistant among the surface treatment combinations tested. The samples with applied coating require renovation after two years of weathering to maintain their original appearance.

Supplementary Materials: The following supporting information can be downloaded at: <https://www.mdpi.com/article/10.3390/f14030440/s1>, Table S1: The images of the samples before the exposure to natural weathering and the images of samples taken in each monitoring period; Table S2: The results of visual assessment of cracking by month of inspection; Table S3: The results of visual assessment of flaking by month of inspection; Table S4: The results of visual assessment of disfigurements caused by fungal or algal growth by month of inspection.

Author Contributions: Conceptualization, J.Ž.; methodology, J.Ž. and M.P.; validation, J.Ž. and M.P.; formal analysis, J.Ž.; investigation, J.Ž.; resources, J.Ž. and M.P.; data curation, J.Ž.; writing—original draft preparation, J.Ž.; writing—review and editing, J.Ž. and M.P.; visualization, J.Ž. All authors have read and agreed to the published version of the manuscript.

Funding: The authors acknowledge the financial support from the Slovenian Research Agency (research programs funding No. P4-0015, “Wood and lignocellulosic composites”, and No. P4-0430, “Forest-wood value chain and climate change: transition to circular bioeconomy”).

Data Availability Statement: The data presented in this study are archived by the corresponding author and can be provided upon written request to the corresponding author.

Conflicts of Interest: The authors declare no conflict of interest.

References

1. Prieto, J.; Kiene, J. *Wood Coatings: Chemistry and Practice*, 1st ed.; Vincentz Network GmbH & Co. KG: Hanover, Germany, 2018; 396p.
2. Resi Kerdiati, N.L.K. Understanding wood finishing using the japanese wood burning technique (Shou Sugi Ban) in architecture. *J. Aesthet. Des. Art Manag.* **2021**, *1*, 15–23.
3. Ebner, D.H.; Barbu, M.-C.; Klaushofer, J.; Čermák, P. Surface modification of spruce and fir sawn-timber by charring in the traditional japanese method—Yakisugi. *Polymers* **2021**, *13*, 1662. [[CrossRef](#)]
4. Čermák, P.; Dejmal, A.; Paschová, Z.; Kymäläinen, M.; Dömény, J.; Brabec, M.; Hess, D.; Rautkari, L. One-sided surface charring of beech wood. *J. Mater. Sci.* **2019**, *54*, 9497–9506. [[CrossRef](#)]
5. Roberts, A.F. The heat of reaction during the pyrolysis of wood. *Combust. Flame* **1971**, *17*, 79–86. [[CrossRef](#)]
6. Richtel, F.; Atreya, A.; Kotsovinos, P.; Rein, G. The effect of chemical composition on the charring of wood across scales. *Proc Combust. Inst.* **2019**, *37*, 4053–4061. [[CrossRef](#)]
7. Yang, L.; Wang, Y.; Zhou, X.; Dai, J.; Deng, Z. Experimental and numerical study of the effect of sample orientation on the pyrolysis and ignition of wood slabs exposed to radiation. *J. Fire Sci.* **2012**, *30*, 211–223. [[CrossRef](#)]
8. Machová, D.; Oberle, A.; Zárybnická, L.; Dohnal, J.; Šeda, V.; Dömény, J.; Vacenovská, V.; Kloiber, M.; Pěňčík, J.; Tippner, J.; et al. Surface characteristics of one-sided charred beech wood. *Polymers* **2021**, *13*, 1551. [[CrossRef](#)]
9. Frangi, A.; Fontana, M. Charring rates and temperature profiles of wood sections. *Fire Mater.* **2003**, *27*, 91–102. [[CrossRef](#)]
10. Kwon, S.-M.; Kim, N.-H.; Cha, D.-S. An investigation on the transition characteristics of the wood cell walls during carbonization. *Wood Sci. Technol.* **2009**, *43*, 487–498. [[CrossRef](#)]
11. Zachar, M.; Čebalová, I.; Kačíková, D.; Zacharová, L. The effect of heat flux to the fire-technical and chemical properties of spruce wood (*Picea abies* L.). *Materials* **2021**, *14*, 4989. [[CrossRef](#)]
12. Czimeczik, C.I.; Preston, C.M.; Schmidt, M.W.I.; Werner, R.A.; Schulze, E.D. Effects of charring on mass, organic carbon, and stable carbon isotope composition of wood. *Org. Geochem.* **2002**, *33*, 1207–1223. [[CrossRef](#)]

13. Morozovs, A.; Laiveniece, L.; Lubinskis, V. Wood one-side surface charring of timber for claddings or recycled wood. In Proceedings of the 20th International Scientific Conference Engineering for Rural Development, Jelgava, Latvia, 26–28 May 2021; pp. 994–1002. [[CrossRef](#)]
14. Baroudi, D.; Ferrantelli, A.; Li, K.Y.; Hostikka, S. A thermomechanical explanation for the topology of crack patterns observed on the surface of charred wood and particle fibreboard. *Combust. Flame* **2017**, *182*, 206–215. [[CrossRef](#)]
15. Byrne, C.E.; Nagle, D.C. Carbonization of wood for advanced materials applications. *Carbon* **1991**, *35*, 259–266. [[CrossRef](#)]
16. Gospodinova, D.; Dineff, P. New surface charred wood effects for charcoal coating, graphic image and drawing. In Proceedings of the 11th Electrical Engineering Faculty Conference (BulEF), Varna, Bulgaria, 11–14 September 2019. [[CrossRef](#)]
17. Li, G.; Gao, L.; Liu, F.; Qiu, M.; Dong, G. Quantitative studies on charcoalification: Physical and chemical changes of charring wood. *Fundam. Res.* **2022**, *in press*. [[CrossRef](#)]
18. Kim, M.J.; Kim, S.; Kim, C.-K.; Shim, K.B. Determination of charring thickness of wood by residual strength analysis. *Bioresources* **2022**, *17*, 1485–1493. [[CrossRef](#)]
19. Wang, Y.; Zhang, Z.; Fan, H.; Wang, J. Wood carbonization as a protective treatment on resistance to wood destroying fungi. *Int. Biodeterior. Biodegrad.* **2018**, *129*, 42–49. [[CrossRef](#)]
20. Buksans, E.; Laiveniece, L.; Lubinskis, V. Solid wood surface modification by charring and its impact on reaction to fire performance engineering for rural development. In Proceedings of the 20th International Scientific Conference Engineering for Rural Development, Jelgava, Latvia, 26–28 May 2021; pp. 899–905. [[CrossRef](#)]
21. Ebner, D.; Stelzer, R.; Barbu, M.C. Study of wooden surface carbonization using the traditional japanese yakisugi technique. *Pro Ligno* **2019**, *15*, 278–283.
22. Yuan, S.; Sun, X.; Wang, W.; Zhou, B.; Sun, X.; Sun, J.; Wang, X. The reaction-to-fire performance of wood covered with a transparent film: A potential method for the preservation of chinese wooden historical buildings. *Int. J. Arch. Herit.* **2022**. [[CrossRef](#)]
23. Peterson, C.J.; Gerard, P.D.; Wagner, T.L. Charring does not affect wood infestation by subterranean termites. *Entomol. Exp. Appl.* **2008**, *126*, 78–84. [[CrossRef](#)]
24. Kampe, A.; Pfriem, A. A note on artificial weathering of spruce (*Picea abies*) with a carbonised layer. *Int. Wood Prod. J.* **2018**, *9*, 86–89. [[CrossRef](#)]
25. Kymäläinen, M.; Hautamäki, S.; Lillqvist, K.; Segerholm, K.; Rautkari, L. Surface modification of solid wood by charring. *J. Mater. Sci.* **2017**, *52*, 6111–6119. [[CrossRef](#)]
26. Kymäläinen, M.; Turunen, H.; Čermák, P.; Hautamäki, S.; Rautkari, L. Sorption-related characteristics of surface charred spruce wood. *Materials* **2018**, *11*, 2083. [[CrossRef](#)] [[PubMed](#)]
27. Šeda, V.; Machová, D.; Dohnal, J.; Dömény, J.; Zárybnická, L.; Oberle, A.; Vacenovská, V.; Čermák, P. Effect of one-sided surface charring of beech wood on density profile and surface wettability. *Appl. Sci.* **2021**, *11*, 4086. [[CrossRef](#)]
28. Kymäläinen, M.; Lourençon, T.V.; Lillqvist, K. Natural weathering of soft- and hardwoods modified by contact and flame charring methods. *Eur. J. Wood Wood Prod.* **2022**, *80*, 1309–1320. [[CrossRef](#)]
29. Kymäläinen, M.; Sjökvist, T.; Dömény, J.; Rautkari, L. Artificial weathering of contact-charred wood—The effect of modification duration, wood species and material density. *Materials* **2022**, *15*, 3951. [[CrossRef](#)]
30. Sohbatzadeh, F.; Shabannejad, A.; Ghasemi, M.; Mahmoudsani, Z. Deposition of halogen-free flame retardant and water-repellent coatings on firewood surfaces using the new version of DBD. *Prog. Org. Coat.* **2021**, *151*, 106070. [[CrossRef](#)]
31. Hasburgh, L.E.; Zelinka, S.L.; Bishell, A.B.; Kirker, G.T. Durability and fire performance of charred wood siding (Shou Sugi Ban). *Forests* **2021**, *12*, 1262. [[CrossRef](#)]
32. *SIST EN 927-3*; Paints and Varnishes—Coating Materials and Coating Systems for Exterior Wood—Part 3: Natural Weathering Test. European Committee for Standardization: Brussels, Belgium, 2019.
33. Schmid, J.; Klippel, M.; Viertel, M.; Presl, R.; Fahrni, R.; Totaro, A.; Frangi, A. Charring of timber—determination of the residual virgin cross section and charring rates. In Proceedings of the World Conference on Timber Engineering, Santiago, Chile, 24–27 August 2020.
34. Du Noüy, P.L. An interfacial tensiometer for universal use. *J. Gen. Physiol.* **1925**, *7*, 625–631. [[CrossRef](#)]
35. Hertz, H.R. Über die Berührung fester elastischer Körper. *J. Die Reine Angew. Math.* **1881**, *92*, 156–171. [[CrossRef](#)]
36. Kretschmann, D.E. Mechanical properties of wood. In *Wood Handbook—Wood as an Engineering Material*; Forest Products Laboratory: Madison, WI, USA, 2010; pp. 1–46.
37. *SIST EN ISO 2810*; Paints and Varnishes—Natural Weathering of Coatings—Exposure and Assessment. European Committee for Standardization: Brussels, Belgium, 2020.
38. *SIST ISO 4628-4*; Paints and varnishes—Evaluation of Degradation of Coatings—Designation of Quantity and Size of Defects, and of Intensity of Uniform Changes in Appearance—Part 4: Assessment of Degree of Cracking. International Organization for Standardization: Geneva, Switzerland, 2016.
39. *SIST ISO 4628-5*; Paints and varnishes—Evaluation of Degradation of Coatings—Designation of Quantity and Size of Defects, and of Intensity of Uniform Changes in Appearance—Part 5: Assessment of Degree of Flaking. International Organization for Standardization: Geneva, Switzerland, 2016.
40. *SIST EN ISO 16492*; Paints and Varnishes—Evaluation of the Surface Disfigurement Caused by Fungi and Algae on Coatings. European Committee for Standardization: Brussels, Belgium, 2014.

41. Corbalán, M.; Millán, M.S.; Yzue, M.J. Color pattern recognition with CIELAB Coordinates. *Opt. Eng.* **2002**, *41*, 130–138. [[CrossRef](#)]
42. Gašparík, M.; Karami, E.; Sethy, A.K.; Das, S.; Kytka, T.; Paukner, F.; Gaff, M. Effect of freezing and heating on the screw withdrawal capacity of Norway spruce and European larch wood. *Constr. Build. Mater.* **2021**, *303*, 124457. [[CrossRef](#)]
43. Buchelt, B.; Wagenführ, A. Evaluation of colour differences on wood surfaces. *Eur. J. Wood Prod* **2012**, *70*, 389–391. [[CrossRef](#)]
44. Guo, Y.; Bustin, R.M. FTIR spectroscopy and reflectance of modern charcoals and fungal decayed woods: Implications for studies of inertinite in coals. *Int. J. Coal Geol.* **1998**, *37*, 29–53. [[CrossRef](#)]
45. Traoré, M.; Kaal, J.; Martínez Cortizas, A. Application of FTIR spectroscopy to the characterization of archeological wood. *Spectrochim. Acta Part A Mol. Biomol. Spectrosc.* **2016**, *153*, 63–70. [[CrossRef](#)]
46. Tintner, J.; Preimesberger, C.; Pfeifer, C.; Soldo, D.; Ottner, F.; Wriessnig, K.; Rennhofer, H.; Lichtenegger, H.; Novotny, E.H.; Smidt, E. Impact of pyrolysis temperature on charcoal characteristics. *Ind. Eng. Chem. Res.* **2018**, *57*, 15613–15619. [[CrossRef](#)]
47. Dias, A.F.J.; Nunes de Oliveira, R.; Deglise, X.; Dias de Souza, N.; Otávio Brito, J. Infrared spectroscopy analysis on charcoal generated by the pyrolysis of *Corymbia citriodora* wood. *Matéria* **2019**, *24*, 7. [[CrossRef](#)]
48. Michell, A.J. FTIR spectroscopic studies of the reactions of wood and of lignin model compounds with inorganic agents. *Wood Sci. Technol.* **1993**, *27*, 69–80. [[CrossRef](#)]
49. Pandey, K.K. A study of chemical structure of soft and hardwood and wood polymers by FTIR spectroscopy. *J. Appl. Polym. Sci.* **1999**, *71*, 1969–1975. [[CrossRef](#)]
50. Pánek, M.; Kubovský, I.; Oberhofnerová, E.; Štěrbová, I.; Niemz, P.; Osvald, A.; Kačík, F. Influence of natural weathering on the ignition and relative burning rate of selected softwoods. *Constr. Build. Mater.* **2021**, *304*, 124615. [[CrossRef](#)]
51. Constantine, M.; Mooney, S.; Hibbert, B.; Marjo, C.; Bird, M.; Cohen, T.; Forbes, M.; McBeath, A.; Rich, A.; Stride, J. Using charcoal, ATR FTIR and chemometrics to model the intensity of pyrolysis: Exploratory steps towards characterising fire events. *Sci. Total Environ.* **2021**, *783*, 147052. [[CrossRef](#)]
52. Li, G.; Hse, C.; Qin, T. Wood liquefaction with phenol by microwave heating and FTIR evaluation. *J. For. Res.* **2015**, *26*, 1043–1048. [[CrossRef](#)]
53. Liu, X.Y.; Timar, M.C.; Varodi, A.M.; Sawyer, G. An investigation of accelerated temperature-induced ageing of four wood species: Colour and FTIR. *Wood Sci. Technol.* **2017**, *51*, 357–378. [[CrossRef](#)]
54. Esteves, B.; Velez Marques, A.; Domingos, I.; Pereira, H. Chemical changes of heat treated pine and eucalypt wood monitored by FTIR. *Maderas-Cienc. Tecnol.* **2013**, *15*, 245–258. [[CrossRef](#)]
55. Nishimiya, K.; Hata, T.; Imamura, Y.; Ishihara, S. Analysis of chemical structure of wood charcoal by X-ray photoelectron spectroscopy. *J. Wood Sci.* **1998**, *44*, 56–61. [[CrossRef](#)]
56. Evans, P.D.; Cullis, I.; Kim, J.D.W.; Leung, L.H.; Hazneza, S.; Heady, R.D. Microstructure and mechanism of grain raising in wood. *Coatings* **2017**, *7*, 135. [[CrossRef](#)]
57. Kymäläinen, M.; Turunen, H.; Rautkari, L. Effect of weathering on surface functional groups of charred norway spruce cladding panels. *Forests* **2020**, *11*, 1373. [[CrossRef](#)]
58. Leikanger Friquin, K. Material properties and external factors influencing the charring rate of solid wood and glue-laminated timber. *Fire Mater.* **2011**, *35*, 303–327. [[CrossRef](#)]
59. Žlahtič, M.; Humar, M. Influence of artificial and natural weathering on the moisture dynamic of wood. *Bioresources* **2017**, *12*, 117–142. [[CrossRef](#)]

Disclaimer/Publisher’s Note: The statements, opinions and data contained in all publications are solely those of the individual author(s) and contributor(s) and not of MDPI and/or the editor(s). MDPI and/or the editor(s) disclaim responsibility for any injury to people or property resulting from any ideas, methods, instructions or products referred to in the content.